Composites Part B 233 (2022) 109631

Contents lists available at ScienceDirect

Composites Part B

journal homepage: www.elsevier.com/locate/composites

Pseudo-ductile effects in ±45° angle-ply CFRP laminates under uniaxial loading: Compression and cyclic tensile test

M.C. Serna Moreno *, S. Horta Muñoz

Universidad de Castilla-La Mancha, Escuela de Ingeniería Industrial y Aeroespacial de Toledo, Instituto de Investigación Aplicada a la Industria Aeronáutica, Av. Carlos III, Real Fábrica de Armas, 45004 Toledo, Spain

ARTICLE INFO

Keywords:
A. Carbon fibre
B. Damage tolerance
C. Laminate mechanics
D. Mechanical testing

ABSTRACT

The capacity of symmetric ±45° angle-ply laminates of carbon fibre reinforced polymer to hold large strains before final failure is studied in uniaxial tensile and compressive loading. In particular, $[\pm 45]_{2S}$ and $[\pm 45]_{4S}$ laminates are tested under tension and compression respectively. Both present a three-staged stress–strain response with a first linear evolution followed by a plateau and a final strain hardening. Thanks to the Loading–Unloading–Reloading tensile test, the pseudo-ductile process is analysed in terms of the strain energy. In the first two stages the percentage of the total energy recovered in each cycle follows a similar correlation than the relation of the apparent tensile stiffness with the initial one. Therefore, assuming a similar pattern in both tensile and compressive loading cases, the mechanical response during the linear and plateau stages undergoes a progressive damage with a stiffness reduction related to the dissipated energy. However, a damage model that includes the influence of the fibre's reorientation would not predict the re-stiffening of the third stage. In this work the last stage of strain hardening is assumed to follow a different pattern because of the microstructural changes of the matrix during the plateau stage. These are promoted by strain localisation processes both under tension and compression, with dimensional changes in perpendicular to the loading direction that are observed thanks to the strain fields obtained by Digital Image Correlation. Finally, the main differences between both loading cases are evidenced with the help of the final failure modes.

1. Introduction

In laminates consisting of polymeric plies reinforced with unidirectional fibres, pseudo-ductility might be defined as the capacity of the composite to hold high strain before final failure. This effect is the result of damage mechanisms and microstructural changes of the matrix combined with the reorientation of the fibres. The phenomenon has raised a significant interest due to the ability to avoid the inherently brittle behaviour of fibre reinforced polymers, that opens the possibility of an early damage detection leading to a safer structure [1–4].

One of the most important research projects that seeks to increase the strain holding-capacity of composite materials is the HiPerDuCT [5], headed by the University of Bristol and the Imperial College London. It looks for alternatives that lead to a pseudo-ductile behaviour, such as different angle-ply laminates [1,3,6], fragmentation of plies [2], "brick and mortar" architectures [7,8] or hybridisation of thin-plies [4, 9–13]. As well, different kind of testing is performed to analyse the possibilities of pseudo-ductile composites, for example their response under high strain rates [13] or the decrease of notch sensitivity [9,14].

Focusing on angle-ply laminates, the stacking sequences with symmetric ply orientations at ±45° under uniaxial loading present a shear driven behaviour that results in a highly non-linear stress–strain response. In fact, the tensile test of $[\pm 45]_{nS}$ is of great relevance because it constitutes a standard for characterising the shear properties of the lamina [15]. Therefore, for many years the uniaxial tensile response of $[\pm 45]_{nS}$ laminates has been analysed in detail from the numerical, analytical and experimental points of view [1,16–21]. In case of a low number of plies in a symmetric ±45° Carbon Fibre-Reinforced Polymer (CFRP) laminate, three well-known stages could be observed (see Section 3): A nearly linear initial stress–strain relation (Stage I), followed by a plateau in which the strain grows without increase in the stress level (Stage II), and a last region with an apparent strain hardening until the final failure (Stage III). The failure process could be better understood following the work of Sket et al. [17], which investigates tensile tests on $[\pm 45]_{2S}$ laminates observing the damage via X-ray tomography. At the end of Stage I matrix cracking is already detected in the outer plies of the stack. Afterwards, during Stage II, the crack density increases rapidly reaching at the end of the plateau a saturation level in the outer layers. Close to the final failure of the specimen, the density of cracks in the inner plies gets even higher than

* Corresponding author.
E-mail address: MariaCarmen.Serna@uclm.es (M.C. Serna Moreno).

https://doi.org/10.1016/j.compositesb.2022.109631
Received 8 August 2021; Received in revised form 21 December 2021; Accepted 9 January 2022
Available online 22 January 2022

in the outer plies. In the course of Stage III, the high level of fibre reorientation in the loading direction competes with the degradation of the matrix response. The diminution of the secant apparent shear modulus due to matrix damage and plastic deformation is confirmed through cyclic tensile tests with $[\pm 45]_{2S}$ laminates in the research of Herakovich et al. [18] or Troty et al. [19] for CFRP, and also in the work of van Paepegem et al. [20] for the case of a Glass Fibre-Reinforced Polymer (GFRP). These investigations also indicate the importance of taking into account the fibres reorientation in the constitutive models.

Beside the tensile tests, there are few studies in the scientific literature about the pseudo-ductile phenomenon of symmetric ±45° angle-ply laminates under different loading scenarios [21]. The study of Cui et al. [21] performs compressive uniaxial tests to $[\pm 45]_{4S}$ laminates in which a significant level of fibre reorientation is promoted away from the loading direction. The effect of fibre rotation on the measured shear properties is experimentally quantified with the comparison between compressive and tensile tests. Another important remark is the strain rate dependency of the mechanical response. Subsequently, under the consideration of the fibres as a brittle constituent, it is pointed out that the matrix should be the main contributor to the pseudo-ductile response due to the significant viscoelastic effects. Meanwhile, previous work of the authors [22] highlights the pseudo-ductile effects in a $[\pm 45]_{6S}$ laminate under three-point bending tests. A high number of plies is needed in order to avoid the flexural–torsional coupling and to promote the pseudo-ductile response. Thanks to the strains measured by means of the Digital Image Correlation (DIC) technique, different degrees of pseudo-ductility can be observed simultaneously at different positions through the thickness.

The work here presented focuses on the resemblances and differences of the pseudo-ductile response of CFRP laminates in $[\pm 45]_{2S}$ and $[\pm 45]_{4S}$ configurations submitted to uniaxial tension and compression. Both are expected to present non-linear stress–strain evolutions which allow them to hold large strains before final failure [21]. But the quantitative differences derive in dissimilar final failure patterns that are explained with the help of the stress state at the plane of maximum shear stress. In order to better understand the full pseudo-ductile process in the tensile case, Loading-Unloading-Reloading (LUR) testing is proposed for checking if the recovered energy in each cycle could be related to the drop of the secant slope. To the knowledge of the authors, this is the first time that the strain energy in LUR tensile tests is used to estimate precisely the reduction of the apparent stiffness of the CFRP laminates. As well, the degradation of the apparent elastic response is reviewed by means of the Classical Laminated Plate Theory (CLPT) [23], that also permits to take into account the level of fibre reorientation. A one-parameter progressive damage model is proposed to estimate the reduction of the matrix properties during loading. With the intention of analysing and interpreting the intriguing plateau and re-stiffening stages under both loading cases, the first observations of the dimensional changes and strain measurements by means of the DIC system are presented. At the moment, the pseudo-ductile effects are not yet deeply examined in the literature for angle-ply laminates submitted to uniaxial compressive tests. This investigation could lay the groundwork for the description of the phenomenon in compression.

2. Materials and experimental facility

Symmetric ±45° laminates are investigated, composed by layers of unidirectional carbon-fibres IMA-12K pre-impregnated with the epoxy resin M21E from Hexcel™ [24]. The prepreg has a 34% of resin content by weight, while the aerial weight and density of the fibres are 268 g/m^2 and 1.79 g/cm^3 respectively, what results in a fibre volume fraction of 59.2%. Each pre-preg ply presents an orthotropic linear elastic behaviour whose in-plane average properties have been determined in previous research [25–27]. Table 1 shows the in-plane normal and shear elastic moduli in the principal directions of the material as well as the major and minor in-plane Poisson ratios. Please notice that the shear modulus of the pristine material is determined at an applied stress of 12 MPa in order to have an estimation at a loading level before the first LUR cycle.

Table 1
Average elastic properties of a unidirectional ply in principal material directions [25–27].

E_1 (GPa)	E_2 (GPa)	G_{12} (GPa)	ν_{12}	ν_{21}
177.56	11.84	7.76	0.39	0.03

For the monotonic and LUR uniaxial tensile tests, $[\pm 45]_{2S}$ laminates are proposed to be studied because the low number of layers allows obtaining a highly non-linear stress–strain curve with a flat plateau and three well delimited stages. The effect of stacking higher number of plies is to hinder the interlaminar propagation of the in-plane matrix cracking produced during the inelastic stages, leading to a pseudo-ductile response without a clear plateau. However, in the uniaxial compressive tests the configuration $[\pm 45]_{4S}$ is taken into consideration to accomplish the limitations imposed for avoiding the instability of the specimen. The nominal thickness of a single ply is $\Delta = 0.25$ mm. So that, the total thickness of each laminate can be estimated as $h = n\Delta$, being $n = 8$ in the $[\pm 45]_{2S}$ and $n = 16$ in the $[\pm 45]_{4S}$. After employing the hand lay-up technique, the fabrication process goes on applying a curing cycle of 7 bar at 180 °C during 120 min [24] by means of a hydraulic hot-platen press LabEcon 300 from the Fontijne Grotnes Group. For both loading cases, the tensile and the compressive tests, rectangular prismatic specimens are machined with the dimensions shown in Fig. 1. The nominal dimensions of the $[\pm 45]_{2S}$ coupons are $L = 200$ mm, $B = 30$ mm and $D = 100$ mm, while in the $[\pm 45]_{4S}$ specimens are $l = 80$ mm, $b = 15$ mm and $d = 15$ mm. For protection purposes, GFRP tabs with 3 mm thickness are bonded at the end of the samples with an Araldite® 2000 epoxy adhesive. Tests are performed using pneumatic grips in an electromechanical servo-controlled machine from the company Microtest with a maximum load capacity of 50 kN. During loading, a LaVision StrainMaster DIC system is utilised for optical full field measurement of displacements and strains. The main correlation parameters considered are the dimension of the sub-image used in the computation and the step between consecutive facets, while a high accuracy image interpolation applying pyramid levels is utilised. Under tension, the subset and step sizes are 99 × 99 pixels and 32 pixels respectively. In addition, strain gauge rosettes from Kyowa and an axial extensometer from MTS are employed to acquire the local strain states, which average the measurements in an axial length of 5 mm and 25 mm respectively. The DIC observations have to be developed in a different and contiguous area of 40 × 25 mm for avoiding the obstruction of the axial extensometer in the post-process of the pictures. Regarding the uniaxial compressive tests, an anti-buckling fixture based on the Modified D695 standard [28] is designed ad-hoc, including a stabilising base which facilitates the alignment of the system (Fig. 2). In order to perform adequate strain measurements, a window that allows visual inspection for utilising the DIC equipment is here proposed. Under compression the region available for the DIC measurements is 6.5 × 4 mm, being the subset and step sizes are 49 × 49 pixels and 12 pixels respectively. Additionally, an opening in the rear part of the fixture permits to glue a strain rosette on the other face of the specimen for controlling the appearance of instabilities. So that, the presence of curvatures due to buckling is reflected in strain measurements with opposite sign on each of the instrumented surfaces.

3. Analytical background

For supporting the evaluation and explanation of the experimental results, four analytical approaches are applied. Energetic considerations based on the energy density obtained from the stress–strain curve are utilised. In addition, the reorientation of the fibres during the process is calculated in terms of geometrical factors as it is indicated in the

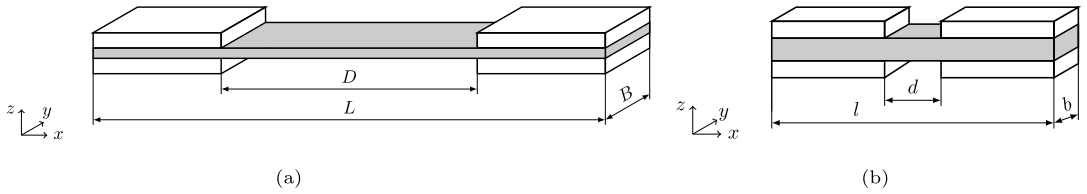

Fig. 1. Dimensions of the coupons. (a) Monotonic and cyclic tensile test. (b) Uniaxial compressive test.

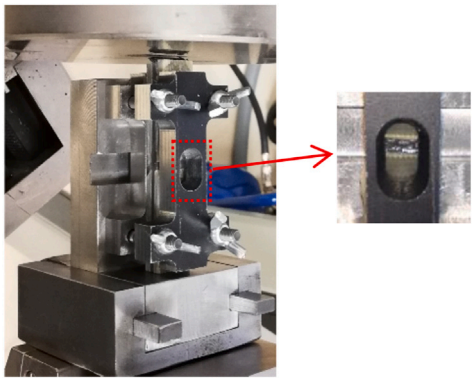

Fig. 2. Modified ASTM D695 fixture [28].

works of Herakovich or Wisnom [16,18]. As well, the degradation of the matrix elastic properties during loading is reviewed with the help of the CLPT [23], that also permits to take into account the level of fibre reorientation. Finally, the basics of the stress analysis are reviewed in order to support the experimental results.

3.1. Strain energy and stiffness reduction

In solid mechanics, the area beneath the stress–strain response obtained from uniaxial testing is the energy per unit volume (energy density) stored in the material during its deformation. Then, the energy dissipation due to damage can be quantified by applying loading cycles up to a predefined load or displacement value. In a LUR cycle, the apparent secant slope ss of a loop can be identified in the representation of the stress–strain response given in Fig. 3. Within the framework of irreversible processes, the energy dissipation might be related to the detriment of the material response and, so that, with the diminution of the apparent secant slope. Therefore, in a LUR test, for a certain cycle the partial area under the stress–strain curve during loading can be defined as w_P (dashed in Fig. 3). This can be related to the total stored energy since the starting point of the full process w_T (shadowed in Fig. 3) by means of the percentage magnitude pw given by Eq. (1). Meanwhile, pss (Eq. (2)) is defined as the percentage of reduction of the secant slope ss with respect to the initial one in the pristine material ss_0 (Fig. 3). The initial secant slope is obtained from the stress–strain evolution before the first LUR cycle, calculating the slope between the points at 8 MPa and 13 MPa. Finally, the tangent slope to the apparent stress–strain response in the loading direction ts is shown in Fig. 3, that will be obtained from the experiments at the Stage I and Stage III of the pseudo-ductile responses of both monotonic loading cases.

$$pw = \frac{w_P}{w_T} 100 \tag{1}$$

$$pss = \frac{ss}{ss_0} 100 \tag{2}$$

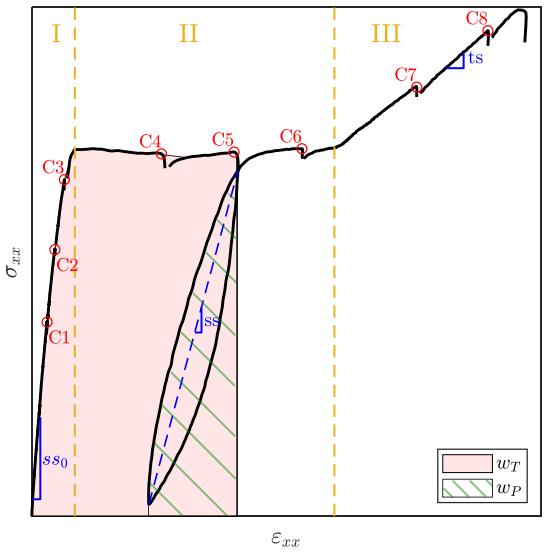

Fig. 3. Example of LUR tensile test in a $[\pm 45]_{2S}$ CFRP laminate and nomenclature utilised. For clarification purpose, only one unloading–reloading cycle is depicted.

3.2. Fibre reorientation in the pseudo-ductile process

The apparent pseudo-ductile response (see example of Fig. 3) is the result of a process of damage and microstructural changes that favour the plasticity in the matrix, combined with the reorientation of the fibres. At the end of Stage I, certain levels of diffuse damage and permanent deformation are already present with some degree of recoverable fibre reorientation. During Stage II, high reorientation of the fibres favoured by large inelastic strain in the polymer are developed. As well, macrocracks in the matrix start to be perceptible in parallel to the fibres. Finally, in Stage III cracks propagate intra- and inter-lamina while the fibres continue their reorientation. Therefore, during the whole loading process the initial fibre angle θ_0 changes due to the so-called "scissoring action". Following the approaches taken by other researchers [16,18], it is possible to estimate along the test the updated fibre angle θ_f taking into account the geometrical changes depicted in Fig. 4. Focusing on a rectangular portion of a ply with a fibre in its diagonal, the initial angle of the fibre is called θ_0 (Fig. 4(a)) and the final orientation after the deformation is named θ_f (Fig. 4(b)). Both angles can be related to the dimensions of the rectangular shape as $\tan\theta_0 = L_{0y}/L_{0x}$ and $\tan\theta_f = L_{fy}/L_{fx}$. In parallel, the differences between the initial and final lengths in each in-plane direction lead to the normal x-strain ε_{xx} and y-strain ε_{yy}, finding the respective expressions $L_{fx} = L_{0x}(\varepsilon_{xx}+1)$ and $L_{fy} = L_{0y}(\varepsilon_{yy}+1)$. Then, combining the previous equations, it is possible to calculate the updated fibre angle θ_f due to the "scissoring action" using the well-known expression given by Eq. (3).

$$\theta_f = \arctan\left[\tan\theta_0 \left(\frac{1+\varepsilon_{yy}}{1+\varepsilon_{xx}}\right)\right] \tag{3}$$

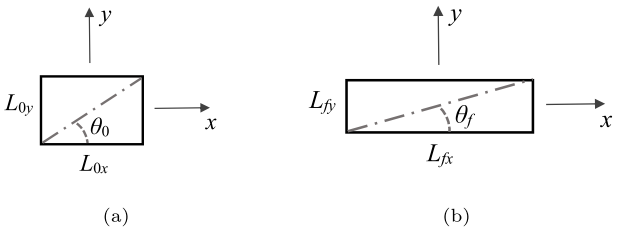

Fig. 4. Geometrical simplification for representing the fibres reorientation. (a) Initial geometry. (b) Deformed shape.

3.3. Reduction of the matrix properties in the CLPT

Many of the models that try to reproduce inelasticity in composites at the mesoscale level describe a first stage of linear response and, from a certain threshold, the beginning of dissipative processes. Generally, it is assumed that if the material is unloaded the stress–strain curve might follow an evolution with a reduced stiffness with respect to the initial one. Then, a series of internal variables could be defined to give an idea of the energy dissipation, referring to its past history and describing its current state. In this scenario, the model presented in this work proposes that the reduction of the material stiffness might be associated to these internal variables. Following the hypothesis and experimental observations from other investigations [18–20], during the pseudo-ductile process of ±45° angle-ply laminates no damage or yielding in the fibres is considered. Consequently, the non-linear evolution would depend only on what happens in the shear and transverse directions to the fibre. Using the traditional ply-stiffness calculation of the CLPT [23], the proposal is to update the elastic properties of the matrix during loading, reducing the transverse modulus E_2 and the in-plane shear modulus G_{12} at the ply-level. Therefore, let us define the internal damage variable ξ whose valid values are in the interval $0 \leq \xi \leq 1$, which would include the reduction of matrix properties along the test due to both damage and plasticity of the polymer. This assumption is similar to the one made by Laux et al. [29], in which a unique parameter is accounted to model numerically the non-linear behaviour of UD composites in shear. Then, the constitutive matrix **Q** of a layer (Eq. (4)) represents the orthotropic relations between the in-plane stresses and the strains at the ply-level in principal material directions. According to the CLPT, once the constitutive matrix is expressed in the in-plane global x and y directions using the updated angle θ_f, the full **ABD** matrix can be assembled computing the membrane stiffness **A**, the membrane-moment stiffness **B** and the moment stiffness **D**. If we name the compliance matrix as $\mathbf{S} = (\mathbf{ABD})^{-1}$, the secant slope ss can be estimated with Eq. (5) taking into account the thickness h of the specimen. This gives an approximation of the apparent axial stiffness that takes into account the reduction of the initial matrix properties and the updated angle of the fibres.

$$\mathbf{Q} = \begin{bmatrix} \frac{E_1}{1-\nu_{12}\nu_{21}} & \frac{\nu_{12}E_2}{1-\nu_{12}\nu_{21}}(1-\xi) & 0 \\ \frac{\nu_{12}E_2}{1-\nu_{12}\nu_{21}}(1-\xi) & \frac{E_2}{1-\nu_{12}\nu_{21}}(1-\xi) & 0 \\ 0 & 0 & 2G_{12}(1-\xi) \end{bmatrix} \tag{4}$$

$$ss = \frac{1}{S_{11}h} \tag{5}$$

3.4. Stress state

Ideal states of uniaxial tension (Fig. 5 top) or uniaxial compression (Fig. 5 bottom) are considered, with either $\sigma_{xx} = \sigma$ or $\sigma_{xx} = -\sigma$ respectively. As the other stress components are $\sigma_{xy} = \sigma_{xz} = \sigma_{yz} = \sigma_{yy} = \sigma_{zz} = 0$, then the x, y and z axes are the principal stress directions. Following the simplification, Mohr's circles let us infer that the maximum value of the shear stress $\tau_{max} = \sigma_{xx}/2$ with a component transverse to the fibre direction $\sigma_\tau = \sigma_{xx}/2$ can be found in a reference system rotated by $\alpha = 45°$ with respect to the x and y in-plane directions (Fig. 5). The standard uniaxial tensile test with ±45° symmetric laminates for characterising the shear properties of the lamina [15] is based on this fact, being the main drawback that a pure shear stress state is not induced in the material.

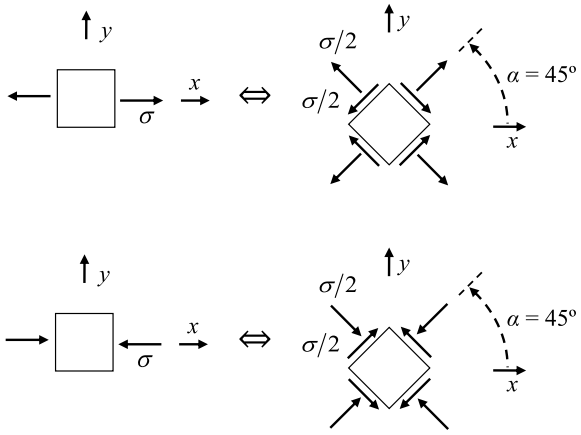

Fig. 5. Equivalence between the stress state at a simplified system aligned with the loading direction and rotated at 45°. Tensile test (top). Compressive test (bottom).

Table 2
Results for the apparent mechanical response of the monotonic tensile loaded $[\pm45]_{2S}$ specimens.

Stage I		Stage II		Stage III	
ts (GPa)	ε_I	$\sigma_{plateau}$ (MPa)	ε_{II}	ts (GPa)	ε_F
19.03 ± 0.27	0.010 ± 0.001	117.51 ± 2.26	0.054 ± 0.002	1.20 ± 0.10	0.101 ± 0.004

4. Experiments, results and discussion

Quasi-static compressive as well as monotonic and LUR tensile tests are developed, in which loading is applied until the moment that the laminate loses its load-carrying capacity. The expected three well-differentiated regions appear in both tests, being the scope of this section to contribute to the state of the art with new observations and to stand out possible similarities and differences.

4.1. Uniaxial monotonic and LUR tensile test

Seven tabbed $[\pm45]_{2S}$ specimens were manufactured, of which four samples were monotonically loaded until failure and three samples were tested with cycles of load, unload and reload (increasing in each reload the maximum displacement achieved in the previous cycle). Table 2 lists the main parameters that describe the mechanical behaviour of the $[\pm45]_{2S}$ laminates under monotonic tension (Fig. 6(a)). It shows the average and standard deviations of the axial strain values at the onset of the plateau ε_I, re-stiffening stage ε_{II} and the final value registered ε_F. The values of ts are obtained as the slope of the stress–strain evolution at the interval of axial strains between 0.1% and 0.3% in Stage I, and between 6.7% and 8.0% in Stage III. The tangent slope in Stage I gives an estimation the elastic modulus of the material. As well, the minimum stress at the plateau $\sigma_{plateau}$ is included. In all the cases the envelope of the cyclic curves followed the strain behaviour of the tensile tests (Figs. 6(a) and 6(b)), corroborating that the full LUR evolutions were adequate.

The usual way to proceed in LUR tests is to establish the level of applied force to be achieved at each unloading–reloading loop [30]. However, the existence of a stress plateau hinders the cycles to be controlled in force during the full test. Then, an ad hoc control program is defined dividing the full test into three phases (Stages I, II and III)

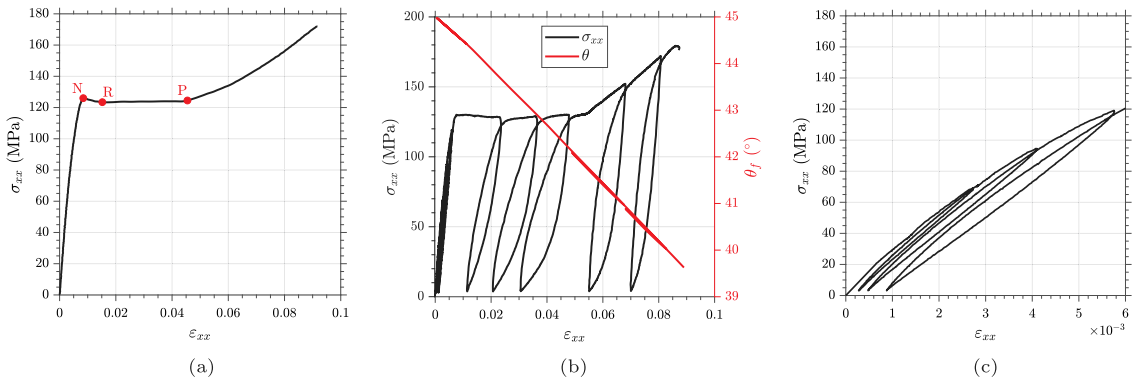

Fig. 6. (a) Tensile test on a representative $[\pm 45]_{2S}$ specimen monotonically loaded, highlighting the points of interest. (b) Full LUR tensile test of a representative $[\pm 45]_{2S}$ laminate: the longitudinal strain ε_{xx} is presented in the horizontal axis, the normal stress σ_{xx} in the left vertical axis and the updated fibre angle θ_f in the right vertical axis. (c) Detail of Stage I in the LUR tensile test.

with a total of 8 cycles (Fig. 3). An initial force-control stage at a rate of 50 N/s is set, in which the upper limits of cycles C1, C2 and C3 are established at ∼ 64 MPa, ∼ 89 MPa and ∼ 116 MPa respectively. A second displacement-control stage with a rate of 1 mm/min is designed, fixing the strains during the plateau in cycles C4 at ∼ 2.3%, C5 at ∼ 3.6% and C6 at ∼ 4.8%. Finally, a third force-control stage at a rate of 50 N/s is proposed to ensure the desired reloading stresses at ∼ 146 MPa and prior to failure at ∼ 164 MPa in cycles C7 and C8 respectively. All the unloads go under the limit of 3.5 MPa. The average strain rate observed in Stage I is $0.47 \cdot 10^{-4}$ s^{-1}, in Stage II it is $3.9 \cdot 10^{-4}$ s^{-1} and, finally, in Stage III it is $2.7 \cdot 10^{-4}$ s^{-1}. Although the differences of strain rates could seem significant, in all the cases they are low enough for avoiding possible viscoelastic effects. This can be confirmed in the work of Cui et al. [21], in which they observe the influence of the strain rate in the stress–strain response of $[\pm 45]_{4S}$ laminates. They utilised a quasi-static strain rate of $5 \cdot 10^{-4}$ s^{-1}, that is higher than the maximum strain rate here observed. Meanwhile they could appreciate the viscoelastic effects at strain rates of $500 \cdot 10^{-4}$ s^{-1}. So that, we consider that during all the test we kept under the hypothesis of quasi-static loading.

The application of this cyclic loading produces the stress–strain curve of a representative specimen depicted in Fig. 6(b), in which a zoom with the detail of the loops in the initial stage is included in Fig. 6(c). The strain gauge rosette is used only for validation purposes at small strain levels because out of them they achieve their measurement limit. So that, the axial extensometer and DIC observations are utilised to collect the strain state of higher magnitude. In the stress–strain response shown in Fig. 6b, an averaged strain in the gauge region is represented in order to avoid as much as possible the local differences of the non-uniform strains measured at different positions during Stage II (Fig. 7). Comparable evolutions are obtained representing the longitudinal strains acquired by means of the axial extensometer and the average value of the DIC axial strains measured in the observed region. Nevertheless, the evolution of the updated angle during tests could be only represented in Fig. 6(b) utilising the DIC measurements. The evolution of the updated angle with the axial strain presents slight changes in the slope.

Table 3 depicts the secant slope ss and the updated angle θ_f found during the three Stages of the LUR tensile test in the $[\pm 45]_{2S}$ laminate of reference. The variable ξ estimates the reduction of the initial matrix properties for obtaining the secant stiffness ss in each cycle taking into account the updated angle of the fibres. ξ increases in Stages I and II, indicating the expected lower matrix properties at higher loads. But please observe how ξ clearly decreases in Stage III, finding an apparent improvement of the matrix response. Evaluating separately the influence of the damage variable and the updated angle, the fibres re-orientation plays a non-negligible role increasing the effective stiffness of the laminate during all the stages, but the apparent global stress–strain evolution is driven by the matrix properties.

Table 3
LUR tensile test in a representative $[\pm 45]_{2S}$ laminate. Updated angle θ_f, secant slope ss and reduction of the matrix properties ξ in Stages I, II and III.

	Stage I			Stage II			Stage III	
	C1	C2	C3	C4	C5	C6	C7	C8
ss (GPa)	26.75	24.89	23.30	9.74	7.53	7.10	11.11	15.32
θ_f (°)	44.87	44.78	44.69	43.70	42.90	42.19	40.97	40.02
ξ (%)	1.30	9.5	16.45	69.68	78.18	80.57	71.63	62.70

Let us start this discussion pointing out the assumption that the matrix should be the main contributor to the non-linear evolution due to the shear driven response of the ±45° angle-plies under uniaxial loading. Thermoset epoxy resins present substantial scale-dependent effects in the stress–strain response [31]. In particular, at the microscale level they behave in a much more ductile manner (including the last stage with an increase of the apparent strength) than large neat resin specimens. In CFRP the reduced size of the matrix region between fibres could facilitate the presence of a non-linear response of the epoxy at the microscale that favours to enter in its plastic regime. Then, following the results of Sui et al. [31], the last stage of strain hardening could be mainly promoted by the transformation in the microstructure of the matrix during Stage II. In semicrystalline polymers this can be induced by a necking process, in which a rearrangement of the polymer chains is favoured by the nature of their bonds [32–34]. Considering the stress–strain evolution of a monotonic tensile test (Fig. 6(a)), the assumption is that at point N a neck initiates. The stress then falls until point R, as the neck is slightly reduced in cross-sectional area. Afterwards, during the region R-P the neck stably propagates along the specimen at a nearly constant stress. The neck spans the full gauge length promoting in the matrix an axial molecular rearrangement with strong bonds dominantly lined up in the load-bearing direction. Subsequently, an upturn in the stress–strain evolution is observed in which the stress increases mainly due to strain hardening of the matrix and the fibres reorientation until fracture occurs.

In order to support this idea, the DIC technique permits to observe the non-uniform longitudinal ε_{xx} and the transversal ε_{yy} strain fields at intermediate loading steps of the plateau (Fig. 7 top). We associate this non-uniform deformation with the necking process, promoted by stress concentrations due to initial geometrical imperfections and/or the proximity of the end-tabs. In an intermediate state of the plateau shown in Fig. 7(b), the transversal strains depict width changes along the gauge length of the specimen of −6.3%. The reader is referred to check the video available in the "Data availability" section to better observe the necking process during the plateau stage. A correlation between the evolution of the strain fields and the transition of the necking along the specimen is schematised in Fig. 7 bottom, in which

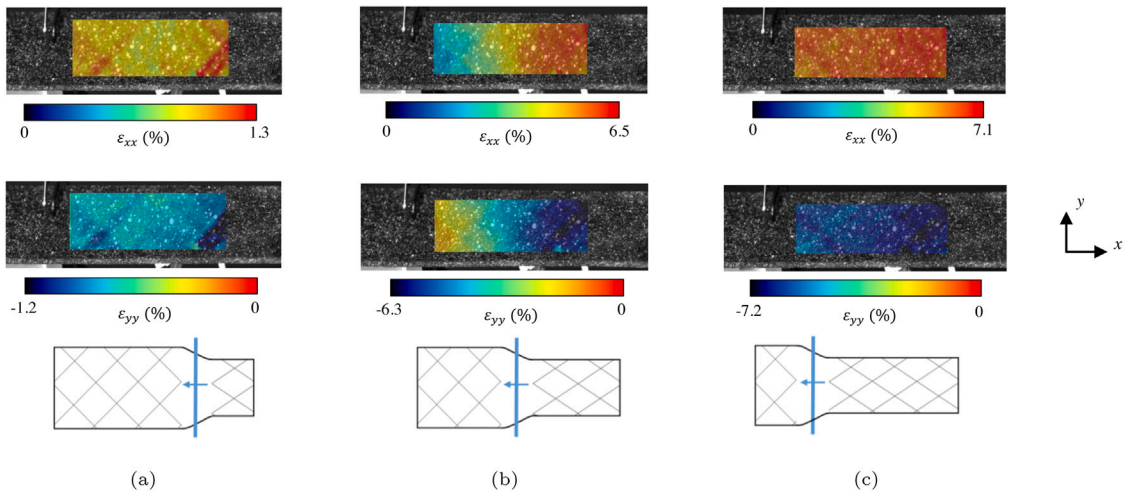

Fig. 7. LUR tensile test of $[\pm 45]_{2S}$ laminate. In Stage II, representation of the ϵ_{xx} and ϵ_{yy} strain fields, as well as sketch of the necking (not to scale). (a) Onset of the plateau. (b) Intermediate state of the plateau. (c) End of the plateau.

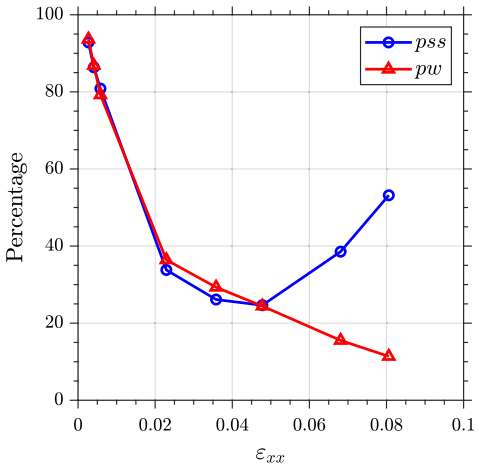

Fig. 8. For a representative LUR tensile test in a $[\pm 45]_{2S}$ laminate, evolution of the *pss* and *pw* values as a function of the strain level ϵ_{xx} at the beginning of each cycle.

a deformed shape with a high scale factor is used for improving its visualisation.

The cyclic tensile test allows us to relate the energy dissipation due to progressive degradation of the matrix with the secant slope observed when the specimen is reloaded after being unloaded. Analysing the response of the material in terms of the secant slope, Table 4 shows the variable *pss* (Eq. (2)) which relates the apparent stiffness in each cycle with respect to the initial one. This brings an estimation of the level of stiffness reduction of the material which should follow a certain correlation with the energy dissipation. With comparative purposes, Table 4 shows the variable *pw* (Eq. (1)) that gives an idea of the recovered energy in each cycle from the total energy accumulated during the full test. In order to show the information more intuitively, in Fig. 8 the values of *pss* and *pw* are plotted as a function of the axial strain level ϵ_{xx} at the beginning of each cycle. It could be highlighted that there is a correlation between the stiffness reduction and the dissipated energy in the first two stages of the stress–strain response, but the correlation is no longer valid at the third stage. This could be related to the mentioned microstructural transformations of the matrix during the plateau.

Table 4
Representative LUR tensile test in a $[\pm 45]_{2S}$ laminate. Correlation between the secant slope percentage (*pss*) and strain energy percentage (*pw*).

	Stage I			Stage II			Stage III	
	C1	C2	C3	C4	C5	C6	C7	C8
pss (%)	92.83	86.36	80.85	33.80	26.13	24.65	38.55	53.18
pw (%)	93.65	86.84	79.22	36.42	29.32	24.42	15.52	11.38

4.2. Uniaxial compressive loading

Different specimens, both tabbed and untabbed, were initially tested in order to obtain a proper stress–strain curve and failure modes under uniaxial compressive loads. Although the use of tabs has been controversial in the specialised field because of some detrimental influence on the measured strength [35], the best results of our testing campaign are obtained using parallelepiped coupons of the laminate $[\pm 45]_{4S}$ with end-tabs (Fig. 1(b)). Then, five quasi-static uniaxial compressive tests are performed at a displacement rate of 1.5 mm/min. All the samples presented the full three-staged stress–strain evolution and in-plane shear failure modes accepted by the standard ISO 14126:1999 [36]. However, two of them exhibited slight additional in-plane kinking bands, that brought small variations in the degree of fibre reorientation and resulted in the change in the slope of the stress–strain evolution at the last stage. Then, the results of the three repetitive tests with comparable failure modes are analysed.

The use of the anti-buckling device allows minimising the instabilities during the test and the strain fields can be acquired by means of the DIC system thanks to the opening in the fixture. A highly non-linear behaviour under compressive loading is found (Fig. 9), observing qualitatively the same three stages as in the uniaxial tensile tests. Table 5 presents the average values and standard deviations of the tangent slopes in Stages I and III, the axial strain value at the onset of the plateau ϵ_I, as well as the minimum stress level $\sigma_{plateau}$ in Stage II. The value of *ts* in Stage I is calculated as the slope of the stress–strain evolution at the interval of axial strains between 0.05% and 0.2%, while in Stage III it is obtained as the slope of a least square regression in this region. Please notice that the axial strain at the onset of the re-stiffening stage is not provided because of the unclear threshold between Stages II and III under compression (Fig. 9). Besides, these specimens did not present a drop in force in which we could identify undoubtedly the rupture value of the measured axial strain.

Comparing the pseudo-ductile response under compression with the tensile stress–strain response of the same $[\pm 45]_{4S}$ laminate reported

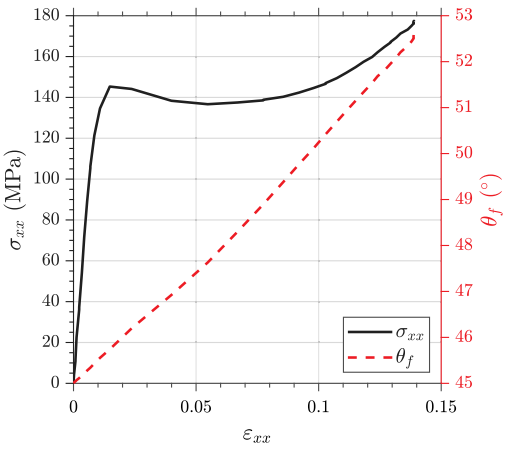

Fig. 9. Representative compressive uniaxial test of a $[\pm 45]_{4S}$ laminate. The longitudinal strain ε_{xx} is presented in the horizontal axis, the normal stress σ_{xx} in the left vertical axis and the updated fibre angle θ_f in the right vertical axis.

Table 5
Results for the apparent mechanical response of the monotonic compressive loaded $[\pm 45]_{4S}$ specimens.

Stage I		Stage II	Stage III
ts (GPa)	ε_I	$\sigma_{plateau}$ (MPa)	ts (GPa)
18.20 ± 0.41	0.015 ± 0.001	137.48 ± 0.71	0.84 ± 0.01

by other researchers [37], similar initial tangent slopes and plateau stresses are developed under tension and compression. But the tangent slope of the Stage III is lower in the compressive tests because of the differences in the reorientation of the fibres and the deformation process. The fibre reorientation is produced in perpendicular to the loading direction with the result of an increase of the initial angle that can be observed in Fig. 9. Moreover, considering the stress–strain evolution of a compressive test (Fig. 9), once the stress peak is achieved at the end of Stage I the stress falls due to the local increase of the cross-sectional area. Subsequently, this "widening effect" spans the full gauge length maintaining approximately the level of stress. This process is expected to promote molecular rearrangements in the matrix that induce the last stage of strain hardening. The increase in width of the cross-sectional area along the region of interest can be intuited from the ε_{xx} and ε_{yy} strain fields shown in Fig. 10 at intermediate loading steps of the plateau. Despite of the visual constrains imposed by the opening of the anti-buckling fixture, a "strain front" spanning the gauge region is observed. Focusing on the intermediate frame of Fig. 10(b), the non-uniform y-strain fields indicate differential changes of 2.3% in the width of the specimen along the visible zone at this instant.

The differences between the tensile and compressive responses become evident in the final failure patterns. The final widening can be intuited in the gauge region of the specimen shown in Fig. 11(a), including a global view of the specimen without the right end-tab for clearer perceiving the dimensional change in the width of the sample. The strain gauge rosette is removed for the picture, letting observe with the naked eye the matrix splitting because of the shear stress component to the fibre direction. As well, high reorientation of the fibres can be distinguished, with a permanent angle of about 52° for compression. Nevertheless, the matrix–fibre interfaces are not separated since the normal stress in the plane of maximum shear stress is compressive (Fig. 5 bottom). The final failure differs in the tensile tests, because the fibres strongly reorient in the loading direction and the stress transverse to the fibres is tensile in the plane of maximum shear stress (Fig. 5 top). As a result, both matrix splitting and transverse matrix cracking are noticeable (Fig. 11(b)). The failure mode exhibits a permanent final fibre angle of about 40° for tension and the in-plane matrix splitting favours the interlaminar debonding, finding clear delaminations in the $+45°/-45°$ interfaces. Due to these differences, the estimation of the shear response of the lamina using ±45° CFRP laminates differs at high strain levels if it is obtained from uniaxial tension or uniaxial compression. Therefore, the existing literature advises to take into consideration the fibre reorientation effects at large strains in order to quantify the true in-plane shear response in the material directions [18–20]. Based on the different failure patterns obtained in the tensile and compressive tests, we would like to add an additional consideration. If the determination of the full non-linear shear response in the material principal directions is sought by means of uniaxial testing with ±45° laminates, the effect of the component transverse to the fibre direction that acts in the plane of maximum shear stress could have a non-negligible influence. Other experimental techniques as the biaxial tensile-compressive experiments in cruciform specimens [25, 38–40] or the test system applied in ISO20337:2018 [41] based on a deformable square-shaped frame can achieve a pure shear state. These testing methods manage to achieve higher levels of ultimate strains and stresses than those in which a transverse component is present. So that, they should be more suitable to determine the pure shear response in principal material directions. Moreover, under the hypothesis that only there would be in-plane shear stresses to the fibres, the response in terms of the stiffness and strength of the lamina should be similar even if the shear stresses have opposite signs [42].

5. Conclusions

The pseudo-ductile mechanical response of ±45° CFRP laminates is studied by means of uniaxial compressive tests in $[\pm 45]_{4S}$ laminates and uniaxial tensile tests in $[\pm 45]_{2S}$ stacking sequences. Both present a three-staged stress–strain response with a first linear evolution followed by a plateau and a final strain hardening. One of the main outcomes of the work comes from the complexity to describe the stress–strain evolution at the last stage referring to the pristine properties of the material. Under both loading cases, the mechanical response in Stages I and II could follow the pattern of a progressive damage with a stiffness reduction related to the dissipated energy. Nevertheless, a damage model would not be able to describe the full three-staged evolution. As well, there is a correlation between the stiffness reduction and the dissipated energy in the first two stages of the stress–strain response, but the correlation is no longer valid at the third stage. Stage III follows a different pattern with an increase of strength and stiffness that suggests microstructural transformations of the resin during Stage II. These microstructural changes are produced in Stage II due to the strain localisation processes both under tension and compression, that are qualitatively and quantitatively observed thanks to DIC strain fields. The non-uniform strain fields show differential width changes along the gauge region at intermediate stages of the plateau. The different stress states induced by the tensile and compressive loading cases are evidenced in the final failure modes. These differences derive in dissimilar final failure patterns that are explained with the help of the stress states at the plane of maximum shear stress. The shear driven process produces in both cases matrix splitting, but visible transverse matrix cracking is only observed under tension followed by clear inter-ply delamination. The transverse stress at high strain levels has a non-negligible influence. Therefore, uniaxial testing with ±45° laminates estimates adequately the in-plane shear response in principal material directions at low strains, but at high strain levels the assessment of the non-linear shear behaviour is clearly affected by the stress transverse to the fibre direction.

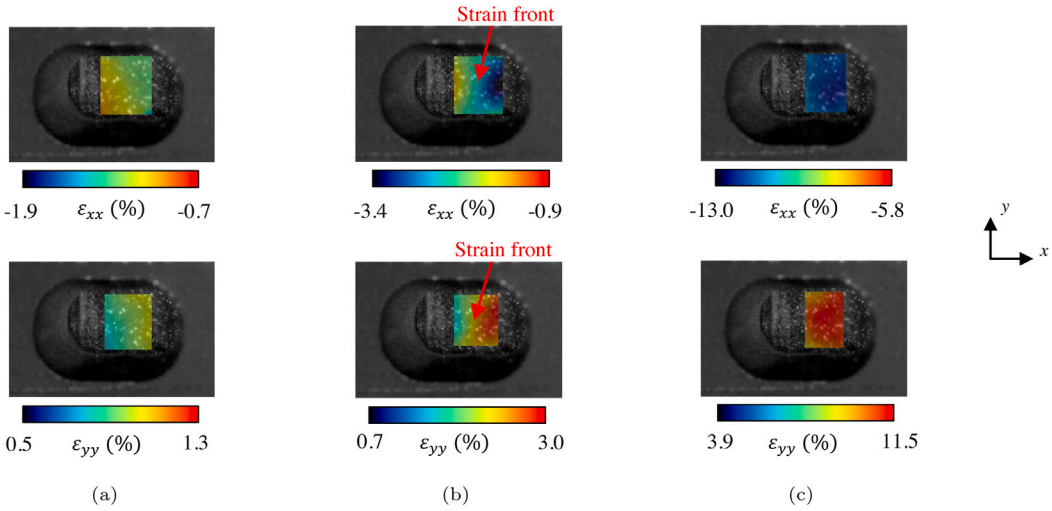

Fig. 10. Compressive test of a $[\pm 45]_{4S}$ laminate. In Stage II, representation of the ϵ_{xx} and ϵ_{yy} strain fields. (a) Onset of the plateau. (b) Intermediate state of the plateau. (c) Last stages of the plateau.

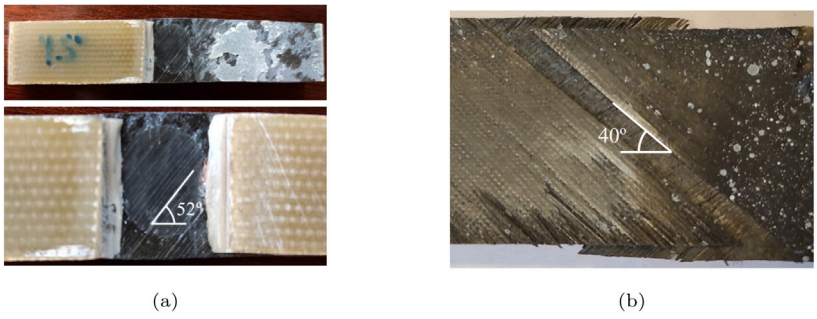

Fig. 11. View of the final crack pattern and permanent reorientation of the fibres. (a) $[\pm 45]_{4S}$ laminate after uniaxial compressive loading, including the view of the specimen after removing the right end-tab. (c) $[\pm 45]_{2S}$ laminate after LUR tensile loading.

CRediT authorship contribution statement

M.C. Serna Moreno: Conceptualization, Funding acquisition, Formal analysis, Investigation, Project administration, Resources, Supervision, Writing – original draft, Writing – review & editing. **S. Horta Muñoz:** Data curation, Investigation, Methodology, Software, Visualization, Writing – review & editing.

Declaration of competing interest

The authors declare that they have no known competing financial interests or personal relationships that could have appeared to influence the work reported in this paper.

Data availability

The video illustrating the necking of the specimen at the plateau stage is available to download from the database: Horta Muñoz, Sergio; Serna Moreno, María del Carmen (2021), "Pseudo-ductile effects in ±45° angle-ply CFRP laminates under uniaxial loading", Mendeley Data, V1, doi:10.17632/ft3jhjhxhs.1. Some or all data or code that support the findings of this study are available from the authors upon reasonable request (email: mariacarmen.serna@uclm.es, email: sergio.horta@uclm.es).

Acknowledgements

The Ministry of Economy and Competitiveness of Spain and the European Regional Development Fund have financially supported this work under the grant DPI2016-77715-R. The publication is part of the project PDC2021-121154-I00, funded by MCIN/AEI/10.13039/501100011033 and by the European Union "NextGenerationEU"/PRTR". In addition, the Government of Castilla-La Mancha should be acknowledged for the regional project SBPLY/19/180501/0000170.

The second author also acknowledges the support provided by the University of Castilla-La Mancha (UCLM), Spain and European Regional Development Fund (ERDF) under the grant 2020/3771. These authors would like to thank the company Airbus for providing the material used in the preparation of the specimens.

References

[1] Fuller JD, Wisnom MR. Pseudo-ductility and damage suppression in thin ply CFRP angle-ply laminates. Compos Part A Appl Sci Manuf 2015;69:64–71. http://dx.doi.org/10.1016/j.compositesa.2014.11.004.

[2] Fuller JD, Jalalvand M, Wisnom MR. Combining fibre rotation and fragmentation to achieve pseudo-ductile CFRP laminates. Compos Struct 2016;142:155–66. http://dx.doi.org/10.1016/j.compstruct.2016.01.073.

[3] Fuller JD, Wisnom MR. Exploration of the potential for pseudo-ductility in thin ply CFRP angle-ply laminates via an analytical method. Compos Sci Technol 2015;112:8–15. http://dx.doi.org/10.1016/j.compscitech.2015.02.019.

[4] Jalalvand M, Czél G, Wisnom MR. Damage analysis of pseudo-ductile thin-ply UD hybrid composites - A new analytical method. Compos Part A Appl Sci Manuf 2015;69:83–93. http://dx.doi.org/10.1016/j.compositesa.2014.11.006.

[5] University of Bristol and Imperial College London. High performance ductile composite technology research project. 2018, http://hiperduct.ac.uk/. [Accessed 10 April 2021].

[6] Fuller JD, Wisnom MR. Ductility and pseudo-ductility of thin ply angle-ply CFRP laminates under quasi-static cyclic loading. Compos Part A - Appl S 2018;107:31–8. http://dx.doi.org/10.1016/j.compositesa.2017.12.020.

[7] Pimenta S, Robinson P. An analytical shear-lag model for composites with "brick-and-mortar" architecture considering non-linear matrix response and failure. Compos Sci Technol 2014;104:111–24. http://dx.doi.org/10.1016/j.compscitech.2014.09.001.

[8] De Luca F, Clancy AJ, R. Carrero N, Anthony DB, De Luca HG, Shaffer MSP, Bismarck A. Increasing carbon fiber composite strength with a nanostructured "brick-and-mortar" interphase. Mater Horiz 2018;5:668–74. http://dx.doi.org/10.1039/C7MH00917H.

[9] Fotouhi M, Jalalvand M, Wisnom MR. Notch insensitive orientation-dispersed pseudo-ductile thin-ply carbon/glass hybrid laminates. Compos Part A - Appl S 2018;110:29–44. http://dx.doi.org/10.1016/j.compositesa.2018.04.012.

[10] Czél G, Wisnom MR. Demonstration of pseudo-ductility in high performance glass/epoxy composites by hybridisation with thin-ply carbon prepreg. Compos Part A - Appl S 2013;52:23–30. http://dx.doi.org/10.1016/j.compositesa.2013.04.006.

[11] Jalalvand M, Czél G, Wisnom MR. Parametric study of failure mechanisms and optimal configurations of pseudo-ductile thin-ply UD hybrid composites. Compos Part A - Appl S 2015;74:123–31. http://dx.doi.org/10.1016/j.compositesa.2015.04.001.

[12] Fotouhi M, Jalalvand M, Wisnom MR. High performance quasi-isotropic thin-ply carbon/glass hybrid composites with pseudo-ductile behaviour in all fibre orientations. Compos Sci Technol 2017;152:101–10. http://dx.doi.org/10.1016/j.compscitech.2017.08.024.

[13] Fotouhi M, Fuller J, Longana M, Jalalvand M, Wisnom MR. The high strain rate tension behaviour of pseudo-ductile high performance thin ply composites. Compos Struct 2019;215:365–76. http://dx.doi.org/10.1016/j.compstruct.2019.02.068.

[14] Czél G, Rev T, Jalalvand M, Fotouhi M, Longana ML, Nixon-Pearson OJ, Wisnom MR. Pseudo-ductility and reduced notch sensitivity in multi-directional all-carbon/epoxy thin-ply hybrid composites. Compos Part A - Appl S 2018;104:151–64. http://dx.doi.org/10.1016/j.compositesa.2017.10.028.

[15] ASTM D3518/D3518M-18. Standard test method for in-plane shear response of polymer matrix composite materials by tensile test of a ±45° laminate. American Society for Testing and Materials; 2018.

[16] Wisnom MR. The effect of fibre rotation in ±45° tension tests on measured shear properties. Composites 1995;26(1):25–32. http://dx.doi.org/10.1016/0010-4361(94)P3626-C.

[17] Sket F, Rodríguez-Hortalá M, Molina-Aldareguía JM, Llorca J, Maire E, Requena G. In situ tomographic investigation of damage development in ±45° carbon fibre reinforced laminates. Mater Sci Tech 2014;31(5):587–93. http://dx.doi.org/10.1179/1743284714y.0000000561.

[18] Herakovich CT, Schroedter RD, Gasser A, Guitard L. Damage evolution in $[\pm 45]_s$ laminates with fiber rotation. Compos Sci Technol 2000;60(15):2781–9. http://dx.doi.org/10.1016/S0266-3538(00)00091-9.

[19] Totry E, Molina-Aldareguía JM, González C, LLorca J. Effect of fiber, matrix and interface properties on the in-plane shear deformation of carbon-fiber reinforced composites. Compos Sci Technol 2010;70(6):970–80. http://dx.doi.org/10.1016/j.compscitech.2010.02.014.

[20] Van Paepegem W, De Baere I, Degrieck J. Modelling the nonlinear shear stress-strain response of glass fibre-reinforced composites. Part I: Experimental results. Compos Sci Technol 2006;66(10):1455–64. http://dx.doi.org/10.1016/j.compscitech.2005.04.014.

[21] Cui H, Thomson D, Pellegrino A, Wiegand J, Petrinic N. Effect of strain rate and fibre rotation on the in-plane shear response of ±45° laminates in tension and compression tests. Compos Sci Technol 2016;135:106–15. http://dx.doi.org/10.1016/j.compscitech.2016.09.016.

[22] Serna Moreno MC, Horta Muñoz S, Romero Gutiérrez A, Rappold C, Martínez Vicente JL, Morales-Rodríguez PA, López Cela JJ. Pseudo-ductility in flexural testing of symmetric ±45° angle-ply CFRP laminates. Compos Sci Technol 2018;156:8–18. http://dx.doi.org/10.1016/j.compscitech.2017.12.015.

[23] Staab GH. Laminar Composites. 2nd edition. Elsevier; 2015.

[24] Hexcel®. HexPly® M21 DataSheet. 2015, Available online at: https://www.hexcel.com/user_area/content_media/raw/HexPly_M21_global_DataSheet.pdf. [Accessed 10 April 2021].

[25] Horta Muñoz S. Complexity of the structural response of fibre reinforced polymer matrix composites. (Ph.D. thesis), Universidad de Castilla-La Mancha; 2020, p. 143, URI http://hdl.handle.net/10578/28223.

[26] Serna Moreno MC, Romero Gutiérrez A, Martínez Vicente JL. Different response under tension and compression of unidirectional carbon fibre laminates in a three-point bending test. Compos Struct 2016;136:706–11. http://dx.doi.org/10.1016/j.compstruct.2015.06.017.

[27] Serna Moreno MC, Romero Gutiérrez A, Martínez Vicente JL. First flexural and interlaminar shear failure in symmetric cross-ply carbon-fibre laminates with different response under tension and compression. Compos Struct 2016;146:62–8. http://dx.doi.org/10.1016/j.compstruct.2016.03.003.

[28] ASTM D695-15. Standard test method for compressive properties of rigid plastics. American Society for Testing and Materials; 2015.

[29] Laux T, Gan KW, Dulieu-Barton JM, Thomsen OT. A simple nonlinear constitutive model based on non-associative plasticity for UD composites: Development and calibration using a Modified Arcan Fixture. Int J Solids Struct 2019;162:135–47. http://dx.doi.org/10.1016/j.ijsolstr.2018.12.004.

[30] Garoz D, Gilabert FA, Sevenois RDB, Spronk SWF, Van Paepegem W. Material parameter identification of the elementary ply damage mesomodel using virtual micro-mechanical tests of a carbon fiber epoxy system. Compos Struct 2017;181:391–404. http://dx.doi.org/10.1016/j.compstruct.2017.08.099.

[31] Sui XM, Tiwari M, Greenfeld I, Khalfin RL, Meeuw H, Fiedler B, Wagner HD. Extreme scale-dependent tensile properties of epoxy fibers. Express Polym Lett 2019;13(11):993–1003. http://dx.doi.org/10.3144/expresspolymlett.2019.86.

[32] Roylance D. Stress-Strain Curves. Department of Materials Science and Engineering, Massachusetts Institute of Technology Cambridge. 2021, https://ocw.mit.edu/. [Accessed 1 November 2021].

[33] Leonov AI. A theory of necking in semi-crystalline polymers. Int J Solids Struct 2002;39(24):5913–26. http://dx.doi.org/10.1016/S0020-7683(02)00478-X.

[34] Breite C, Melnikov A, Turon A, de Morais A, Le Bourlot C, Maire E, Schöberl E, Otero F, Mesquita F, Sinclair I, Costa J, Mayugo JA, Guerrero JM, Gorbatikh L, McCartney L, Hajikazemi M, Mehdikhani M, Mavrogordato M, Camanho P, Tavares R, Spearing SM, Lomov SV, Pimenta S, Van Paepegem W, Swolfs Y. Detailed experimental validation and benchmarking of six models for longitudinal tensile failure of unidirectional composites. Compos Struct 2022;279:114828. http://dx.doi.org/10.1016/j.compstruct.2021.114828.

[35] Adams DF. Tabbed versus untabbed fiber-reinforced composite compression specimens. In: Zureick A, Nettles A, editors. Composite Materials: Testing, Design, And Acceptance Criteria. ASTM International; 2002, p. 3–16. http://dx.doi.org/10.1520/STP10628S.

[36] ISO 14126:1999. Fibre-reinforced plastic composites - Determination of compressive properties in the in-plane direction. International Organization for Standarization; 1999.

[37] Caminero MA, Rodríguez GP, Chacón JM, García-Moreno I. Tensile and flexural damage response of symmetric angle-ply carbon fiber-reinforced epoxy laminates: Non-linear response and effects of thickness and ply-stacking sequence. Polym Compos 2019;40:3678–90. http://dx.doi.org/10.1002/pc.25230.

[38] Serna Moreno MC, Martínez Vicente JL. In-plane shear failure properties of a chopped glass-reinforced polyester by means of traction-compression biaxial testing. Compos Struct 2015;122:440–4. http://dx.doi.org/10.1016/j.compstruct.2014.12.018.

[39] Serna Moreno MC, Horta Muñoz S. Elastic stability in biaxial testing with cruciform specimens subjected to compressive loading. Compos Struct 2020;234:111697. http://dx.doi.org/10.1016/j.compstruct.2019.111697.

[40] Horta Muñoz S, Serna Moreno MC. Numerical modelling of the pseudo-ductility effect in ±45° angle-ply laminates under biaxial loading. In: 18th European Conference On Composite Materials (ECCM18). Athens, Greece; 2018.

[41] ISO 20337:2018. Fibre-reinforced plastic composites - Shear test method using a shear frame for the determination of the in-plane shear stress/shear strain response and shear modulus. International Organization for Standarization; 2018.

[42] Jones RM. Mechanics Of Composite Materials. 2nd edition. Taylor & Francis; 2002.